Soft Matter

PAPER

View Article Online
View Journal | View Issue

Cite this: *Soft Matter*, 2026, **22**, 438

Efficient silicon-containing di-chain anionic surfactants for stabilizing oil–water interfaces in microemulsions

Adhip Rahman,†*[a] Julian Eastoe,*[a] Ilona E. Serafin,[a] Georgina L. Moody,[a] Dania M. Khairuldin,[a] Saachi Sennik,[a] Sarah E. Rogers,[b] Robert M. Dalgliesh[b] and Sylvain Prévost[c]

New di-chain anionic surfactants containing silicon (Si) atoms in the hydrophobic chain-tips (trimethylsilyl (TMS) hedgehog surfactants) are able to reduce air–water (A–W) surface tension γ_{cmc} to as low as ≈22 mN m^{-1} (A. Czajka, C. Hill, J. Peach, J. C. Pegg, I. Grillo, F. Guittard, S. E. Rogers, M. Sagisaka and J. Eastoe, *Phys. Chem. Chem. Phys.*, 2017, **19**, 23869). However, the extent to which these surfactants stabilize alkane oil–water (O–W) interfaces is unexplored. Here, it is shown that such TMS surfactants are able to stabilize water-in-oil microemulsions (W/O-μEs). The O–W interfacial tensions $\gamma_{o/w}$ in these μEs are ultra-low, in the range of 10^{-2} to 10^{-4} mN m^{-1}, and μE-stability can be optimized by varying surfactant and solvent chemical structures. For example, with aliphatic *n*-alkanes and cycloalkanes, the surfactant AOT–SiC alone stabilizes W/O-μEs over a wide temperature window, but not with the aromatic solvent toluene. Likewise, AOT–SiB forms W/O-μEs, but preferably in aromatic solvents, such as toluene. Contrast-variation small-angle neutron scattering (SANS) measurements indicate that the water droplets in these W/O-μEs are stabilized by surfactant-monolayers. In all of these systems, the droplet morphologies and shapes are correlated with the proximity to (from) the μE-phase stability boundaries. The results show that Si-containing TMS surfactants are effective at O–W interfaces, promoting the ultra-low interfacial tensions necessary for stabilization of μEs. These TMS surfactants offer credible alternatives to environmentally damaging and health-hazardous fluorinated surfactants (FSURFs).

Received 11th August 2025,
Accepted 17th November 2025

DOI: 10.1039/d5sm00817d

rsc.li/soft-matter-journal

1. Introduction

In the field of surfactants, the di-chain anionic surfactant aerosol-OT (AOT1, Fig. 1) is an example of a design classic.[1] As such, AOT1 is a very flexible and adaptable surfactant, reducing aqueous surface tension (γ) and interfacial oil–water interfacial tension ($\gamma_{o/w}$) to ultra-low values (see below), micellizing in aqueous and apolar solvents, and stabilizing microemulsions (μEs) and a range of lyotropic liquid crystalline phases.[2–5] In fact, AOT is one key example of a much broader family of related surfactants,[1–5] which have been synthesized and studied to expand the applications of surfactants and explore detailed chemical structure–function relationships. This group of AOT analogues encompass extensive variations in the chemical architecture of the hydrophobic chain fragments, including different linear and branched chain motifs, as well as fully and partially fluorinated chains.[1,2] This latter class of fluorocarbon AOT surfactants (FSURFs) are noteworthy, being especially surface-active and lowering the limiting surface tension at the aqueous critical micelle concentration γ_{cmc} to ≈15–25 mN m^{-1}.[1,2] As a result, FSURFs of this kind are industrially relevant[6] with real and potential applications as lubricants,[7] fire-fighting foams,[8] and pharmaceutical[9] and cosmetic formulations.[10] However, they are now recognized as environmental pollutants with associated health hazards of bioaccumulation and chemical toxicity.[10] These FSURFs come under the general category of perfluoroalkyl substances (PFAS),[8,10–13] which are now under close regulatory scrutiny.[10,13–16] For example, in the US, the production and distribution of certain PFAS are restricted under federal law.[17–19]

Hence, there is a pressing need to find alternatives for PFAS. Unfortunately, this presents a chemical challenge, since only very few non-fluorinated compounds are able to match the

[a] *School of Chemistry, University of Bristol, Cantock's close, BS8 1TS, Bristol, UK. E-mail: rahmanadhip92@gmail.com*
[b] *ISIS Neutron and Muon Facilities, Rutherford Appleton Laboratory, Chilton, Oxon OX11 0QX, UK*
[c] *Institut Laue-Langevin – The European Neutron Source, 71 avenue des Martyrs, CS 20156, 38042 GRENOBLE Cedex 9, France*
† Current address: Biochemistry and Microbiology Department, North South University, Dhaka – 1229, Bangladesh.

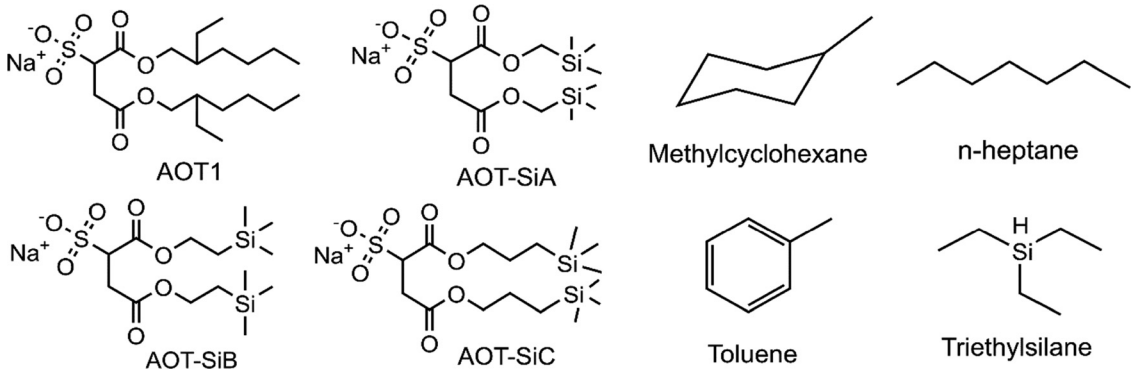

Fig. 1 Chemical structures of the surfactants and solvents.

performance of PFAS and FSURFs.[20–22] The limited subset of surfactants (and polymers) includes certain silicon (Si) containing siloxanes, bearing repeating –Si–O– units.[20–22] In general, siloxane surfactants possess enhanced hydrophobic tail flexibility – owing to the relatively larger (compared to a C atom) Si atom and extended Si–O– moeities.[22] However, silicone surfactants do have limitations for academic research, being difficult to purify and prone to hydrolysis.[21]

Other potential candidates include surfactants containing Si-atoms and trimethyl chain-tips, as first reported by Czajka *et al.*[23] This class was called trimethylsilyl (TMS) hedgehogs (Fig. 1), and it was shown that they can lower γ_{cmc} to $\approx$22–26 mN m^{-1}. In terms of aqueous surface tension reduction, these TMS surfactants, especially AOT–SiC (Fig. 1), outperform any of the hydrocarbon-only AOT-analogues synthesized so far[1] and exhibit comparable γ_{cmc} values to FSURFs.[2] In addition, these TMS surfactants do not contain –Si–O– moieties and hence are expected to be more chemically stable compared to siloxanes. Therefore, such TMS surfactants are credible potential alternatives to FSURFs. Small-angle neutron scattering (SANS) measurements suggested that these Si-surfactants micellize in aqueous solution, forming spherical or ellipsoidal aggregates.[23]

An open question remains, whether or not these TMS surfactants are also effective at oil–water (O–W) interfaces. AOT–SiC was shown to stabilize water–supercritical CO_2 interface,[24] so there is indication that the TMS surfactants may potentially stabilize O–W interfaces in general. However, oily solvents are a broad class of compounds with many chemical variations (Fig. 1); the chain length of the TMS hydrophobic ends is another chemical variable. The link between these two chemical features in stabilizing O–W interfaces is an unexplored area: here, this aspect is addressed. Water-in-oil microemulsions (W/O-μEs) are thermodynamically stable and as such can be considered as model colloidal systems for investigating surfactant monolayers at O–W interfaces over a range of conditions.[25] In μEs, O–W specific surface areas (S/V) are large, and interfacial tension $\gamma_{o/w}$ is considered to be ultralow – of the order of 10^{-2} to 10^{-4} mN m^{-1}.[25,26] The capacity of μEs to disperse water is characterized by the water-to-surfactant molar concentration ratio, W (= [surf]/[water]), and droplet volume fraction ϕ_d (= ϕ_{water} + ϕ_{surf}) using temperature–composition (T–C) phase diagrams. Although nonionic siloxane surfactants were reported to form various types of μEs (water-in-oil, oil-in-water or bicontinuous), not only are those surfactants hydrolytically unstable,[21] but also the phase stability of single-phase (L_2) W/O-μEs is limited.[27–30]

The range of stability and structural and physicochemical properties of W/O-μEs stabilized by the common AOT1 and its wider family of analogues are now well-documented.[4,31–34] For such dilute W/O-μEs, single L_2-phase (W/O droplets) domains can normally be found between two phase-boundaries:[31] a lower-temperature boundary T_L (W/O-μEs in equilibrium with excess water, a so-called Winsor II system) and an upper-temperature boundary T_U (the cloud point with a phase transition to a two-phase system, with a surfactant-rich and a surfactant-poor phase). With common AOT1, the L_2-domain can be tuned towards higher or lower temperature by systematic variation of the chemical structure of the oily solvent.[34] With a given oil, a similar control over phase stability can also be achieved by varying the chemical structure and architecture of the surfactant hydrophobic chains.[4,32,33]

In general, alkyl chain branching in hydrocarbon AOT-analogues is believed to be a key feature facilitating μE-formation,[4,32] and as shown in Fig. 1, the TMS surfactants comprise trimethyl chain-tips. The extent to which this, as well as Si-atom inclusion along the hydrophobic tails, governs surfactant–solvent chemical compatibility and μE formation is explored in this work.

Fig. 1 shows the surfactants and the solvents studied here. The solvents represent examples of linear *n*-alkanes, cycloalkanes and aromatic hydrocarbons. The μE phase behavior was monitored over a wide temperature window (277–348 K) to locate the L_2-domains. O–W interfacial tensions were measured to compare the interfacial properties of the TMS surfactants with the benchmark AOT1. Contrast-variation small-angle neutron scattering (SANS) measurements were carried out to reveal the μE droplet morphology and characterize the interfacial surfactant films. The results indicate that TMS surfactants are effective stabilizers of O–W interfaces and μEs and under certain circumstances may offer viable alternatives to certain PFAS.

2. Materials and methods

2.1 Materials

Chemicals were obtained as follows – 3-trimethylsilyl-1-propanol for AOT–SiC (97%, Sigma-Aldrich), toluene-4-sulfonic acid (Acros), toluene (99%, Fisher), sodium metabisulfite (Alfa Aesar), sodium sulfite (Alfa Aesar), ethanol (99%, Sigma-Aldrich), HCl (35% conc., VWR), Na_2CO_3 (Fisher), anhydrous $MgSO_4$ (Fisher), silica (Merck), diethyl ether (99.5%, Sigma-Aldrich), petroleum ether 40/60 (ACS reagent grade, Sigma-Aldrich), methanol (99.8%, Sigma-Aldrich), TLC plates (silica gel 60 on aluminium plates, Sigma-Aldrich), $KMnO_4$ (Fisher), *n*-heptane (99%, Sigma-Aldrich), *n*-decane (99%, Sigma-Aldrich), toluene (99%, Fisher), methylcyclohexane (99%, Sigma), and triethylsilane (TES 99%, Acros); deuterated solvents: D_2O (99.9%, Cambridge Isotopes), DMSO-d_6 (99.9%, Sigma), $CDCl_3$ (99.8%, Sigma), *n*-heptane-d_{16} (>99.0%, Apollo), *n*-octane-d_{18} (>99.0%, Apollo), methylcyclohexane-d_{14} (>99.5%, Apollo), and toluene-d_8 (99.0%, Sigma). The solvents were used as received. Ultrapure water was used throughout the work (Millipore, 18.2 MΩ cm).

Aerosol-OT (AOT1) was obtained from Sigma-Aldrich (97%) and washed according to the procedure mentioned in SI (Section S.1). The versions of AOT–SiA and AOT–SiB surfactants reported in this work were previously synthesized in-house and were received as white powdery surfactants. Prior to use, these surfactants were purified following procedures mentioned in the SI, Section S.1.

Synthesis and purification of the surfactants were carried out following methods as previously reported.[23] Details of synthesis and characterization are given in Section S.1 of the SI. For preparing W/O-μEs and interfacial tension measurements, ultrapure water was used.

2.2 Methods

a. Phase behavior. Microemulsions (μEs) were formulated in 1 ml volumetric flasks and were held in custom-built phase-behavior racks, which were placed in a Grant LTD6G thermostated water bath. The temperature was increased at intervals of two degrees; at each temperature the systems were equilibrated for 20 minutes, and the samples were gently shaken before visual observation.

b. Interfacial tension. O–W interfacial tension (IFT, $\gamma_{o/w}$) measurements were carried out using a Krüss spinning drop tensiometer (SDT), which is appropriate for the range $\sim 10^0$–10^{-4} mN m^{-1} (details of the procedures in Section S.2 of the SI).

c. Small-angle neutron scattering (SANS). SANS measurements were carried out on either a D33[35] (Institut Laue Langevin – The European neutron Source, Grenoble, France) or Larmor and Sans2d[36] diffractometers (ISIS Neutron and Muon Source, Rutherford Appleton Lab, UK). Measurements were performed at 298.0 (± 0.2) K. Samples were held in either 1 mm path-length (core-contrast samples with h-alkanes) or 2 mm rectangular quartz cells (shell-contrast samples with D_2O and d-alkanes). Site-specific data normalization procedures were employed (using Grasp[37] for D33 and Mantid[38] for Larmor and Sans2D) and model-fitting of the normalized SANS data was carried out using SasView (version 5.0.4, https://www.sasview.org/).[39] Details about the instrument specifications, fitting models and the simultaneous core–shell contrasts are provided in the SI (Section S.3).

3. Results

3.1 Solubility in non-polar solvents

While AOT1 is soluble in a wide range of nonpolar solvents, the TMS surfactants themselves are not. In Fig. 2, photographs of AOT–SiA, AOT–SiB and AOT–SiC with *n*-heptane and toluene are shown: clearly, AOT–SiA and AOT–SiB do not fully dissolve in these solvents, AOT–SiC properly dissolves only in aromatic toluene. As a model cycloalkane solvent, methylcyclohexane was also tested, but again the surfactants were insoluble. After 30 minutes of bath-sonication at 318 K, AOT–SiA and AOT–SiB gave rise to cloudy suspensions in these solvents, but then rapidly phase separated when cooled back to 298 K. On the other hand, AOT–SiC does dissolve in toluene (but not in *n*-heptane or methylcyclohexane) – even at a concentration as high as 0.10 M. In terms of solubility in oils, these surfactants are akin to di-chain cationic dialkyldimethylammonium halide surfactants.[40,41]

As a result of their insolubility, it may be assumed that TMS surfactants do not form ''dry'' reverse micelles (dry RMs, [water]/[surf] or $W = 0$).[42]

3.2 μE phase diagrams

Over a temperature range of 277–333 K, W/O-μEs could not be formed with AOT–SiA in *n*-heptane and methylcyclohexane at [surf] = 0.025 and 0.050 M. However, in toluene, single-phase systems were found at low W values between 2 and 10, at temperatures over 333 K. Nevertheless, the toluene systems were highly temperature-sensitive and upon cooling the surfactant rapidly phase-separated. Fig. 3(a) and (b) show temperature–composition (T–C) phase diagrams of TMS surfactant W/O-μEs with a range of hydrocarbon solvents.

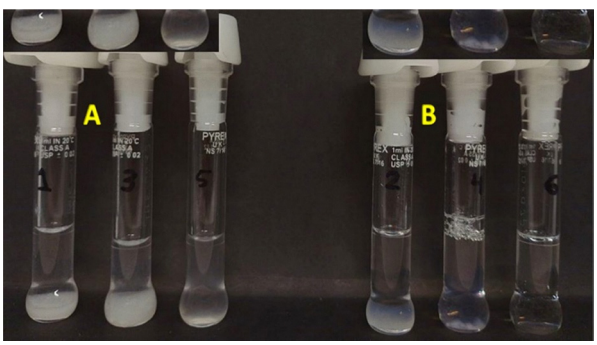

Fig. 2 Appearance of the TMS-surfactants at 0.020 M and 298 K of (left-to-right in each panel) AOT–SiA, AOT–SiB and AOT–SiC in (panel A) *n*-heptane and (panel B) toluene. Images were taken after the samples were sonicated for 30 minutes at 318 K and then left at 298 K for three hours in a water-bath. The upper insets show zoomed-in bottom of the volumetric flasks.

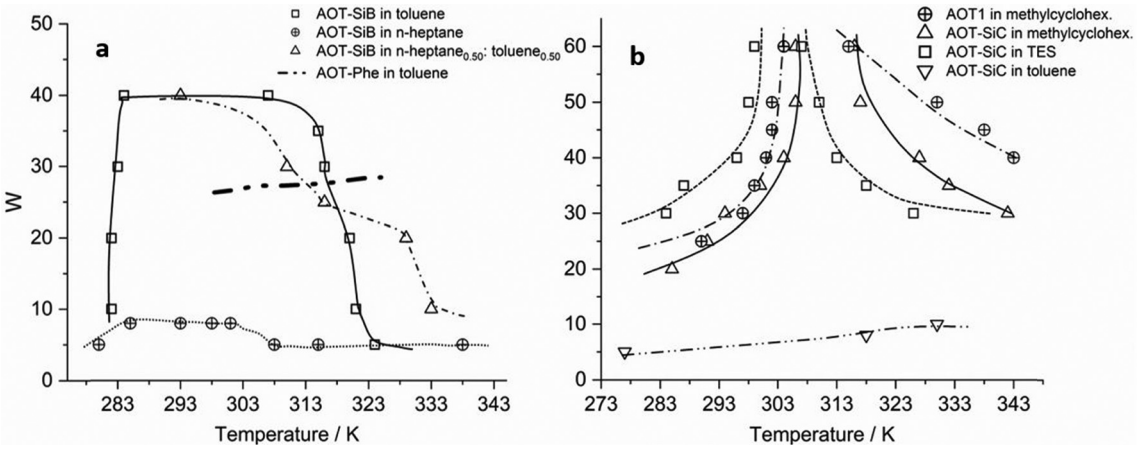

Fig. 3 Temperature–composition (T–C) phase diagrams of (a) AOT–SiB W/O-μEs in toluene, *n*-heptane$_{0.50}$: toluene$_{0.50}$ [mole fraction] and pure *n*-heptane; AOT–Phe W/O-μEs in toluene are shown for comparison (reprinted and adapted from ref. 33 with permission, copyright 2005 American Chemical Society); (b) T–C phase diagrams of AOT–SiC-based W/O-μEs in methylcyclohexane, triethylsilane (TES, Fig. 1) and pure toluene. The phase diagram of AOT1-μEs in methylcyclohexane in (b) is shown for comparison. In (a), the area under each of the dashed curves represents a single-phase L_2-μE. The areas outside the curves represent cloudy phases or surfactant phase separation. In (b), for each pair of the identical dashed curves for AOT–SiC μEs (and for AOT1-μEs), the T_L is represented by the boundary towards lower temperature and T_U towards higher temperature. The curves/lines are a guide to the eyes.

AOT–SiB W/O-μEs in toluene were stable over a reasonably wide temperature window up to $W \approx 40$, above which a surfactant-rich phase separated. Interestingly, the shape of the L_2-domain suggests greater water-loading capacity for AOT–SiB based systems than for the phenyl-tipped dichain hydrocarbon AOT1 analogue, AOT–Phe based W/O-μEs in toluene,[33] which seems to be an advantage of Si-containing surfactants over hydrocarbon surfactants, even containing "polarizable" [Table S3, SI] chain-tips such as phenyl rings. The lower solvent specificity and enhanced microemulsification capacity of AOT–SiB can also be understood, in that it shows a limited μE-domain in a solvent blend containing *n*-heptane, while AOT–Phe does not microemulsify in *n*-heptane at all.[33]

As can be seen, AOT–SiC forms W/O-μEs in *n*-heptane (Fig. S2 in the SI), which somewhat resembles AOT1-based W/O-μEs in *n*-decane.[34,43] W/O-μE formation was also attempted in *n*-decane, and at 298 K, a T_U phase separation was observed at $W \approx 9$. Like AOT1-based W/O-μEs in linear *n*-alkanes,[34] the T_U boundaries of AOT–SiC W/O-μEs shift to lower temperature upon increasing the alkane solvent chain length. As Fig. 3(b) shows, AOT–SiC W/O-μEs do form in methylcyclohexane and a model Si-containing nonpolar solvent triethylsilane, TES. Note that the AOT–SiC tails and TES contain an equal number of C and Si-atoms. Moreover, the phase boundaries and L_2-domain for the latter somewhat resembles AOT1-μEs in *n*-heptane (Fig. S2).

Previously, Si-containing nonionic silicone surfactants (bearing –Si–O–Si– repeat units) were studied as microemulsifiers.[29,30,44,45] The phase diagrams of silicone surfactants/oils/water ternary systems revealed only narrow W/O-μE regions and high temperature-sensitivity, and only at relatively high surfactant concentrations (~20 wt%), so that it cannot be claimed that these are dilute W/O-μEs. Steytler *et al.*[46] reported the T–C phase diagrams for silicone-surfactant based W/cyclohexane μEs at low surfactant content. However, the L_2-domain was limited in terms of both W and the upper temperature limits ($W < 30$, $T_U < 318$ K). In comparison, the anionic TMS-derivatives studied here, in particular AOT–SiC based systems, are better for W/O-μEs, offering stability over a wider class of solvents and temperatures than such nonionic silicone surfactants.

3.3 O–W interfacial tension ($\gamma_{o/w}$)

The general O–W interfacial tension profiles (O–W IFT, $\gamma_{o/w}$) for Winsor transitions (WI → WIII → WII) of AOT-based μEs as a function of [NaCl] have been introduced elsewhere.[4,47] The sections of the $\gamma_{o/w}$ profiles shown here (Fig. 4(a) and (b)) are from the high salt branch[4,47] of the Winsor II μE region (or WII – corresponding to W/O-μEs in equilibrium with excess water). For AOT–SiB and AOT–SiC, the solvent-specific patterns of interfacial tension behavior echo those seen for phase behavior, in terms of the microemulsifying capacity, that is, a higher W_{max} at 298 K, and the shift of the L_2-μEs towards the lower temperature for a given series of composition corresponds to the very low $\gamma_{o/w}$ values [$\sim 10^{-4}$ mN m^{-1}][26,47] (Fig. 3(a) and (b)).

Example $\gamma_{o/w}$ profiles for the AOT1-based systems are also included here for comparison purposes. In general, the trends are dominated by the oil chain chemical structure, for AOT–SiB the water–*n*-heptane $\gamma_{o/w}$ profile is an outlier (*i.e.*, lowering of $\gamma_{o/w}$ upon increasing [NaCl]). This profile is rather reminiscent of Winsor I (WI)-μEs (oil-in-water, O/W),[47] suggesting that AOT–SiB does not partition very well into *n*-heptane.

The $\gamma_{o/w}$ profiles for AOT–SiB are consistent with more favorable partitioning into toluene compared to AOT–SiC and AOT1, again being in line with progressions in μE-phase behavior of these surfactants in toluene. An interesting observation involves the overlap of the $\gamma_{o/w}$ profiles corresponding to AOT1 at water [NaCl]–*n*-decane and AOT–SiC at

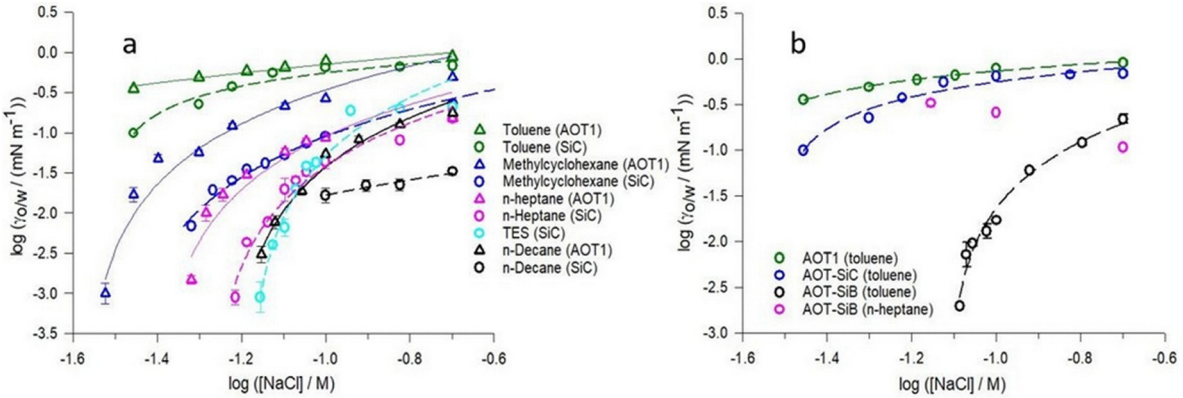

Fig. 4 (a) [NaCl]-scan profiles of oil–water interfacial tensions $\gamma_{o/w}$ in the WII-μE phase region. AOT1-based systems are shown for comparison purposes. Panel (b) emphasizes the $\gamma_{o/w}$ reduction of AOT–SiB on the water/toluene interface and compares AOT–SiB with AOT1 and AOT–SiC. The lines are a guide to the eyes.

water [NaCl]–*n*-heptane interfaces. As discussed earlier for these two systems, the phase-boundaries were close to each other, and below in Section 3.4 it will be shown that the SANS profiles also share common features.

3.4 SANS

a. Droplet morphology. The phase behavior study presented above showed that AOT–SiC forms W/O-μEs in a range of solvents, while AOT–SiB forms μEs in toluene, and so the SANS profiles discussed in this section involve these two surfactants. The phase behavior as well as IFT measurements show similarities between these Si-containing surfactants, regular hydrocarbon AOT1 and numerous related analogues, in terms of W/O-μE formation.[4,26,32,33] Hence, it is of interest to understand the local structures of these interfaces in detail. In Fig. 5, core-contrast (droplet-cores contain deuterated water, D_2O/h-surf/h-oil: D/H/H) SANS profiles of AOT–SiC W/O-μEs are shown in three different solvents. Extensive fitting trials suggested that these profiles conformed with a spherical model-fit, including a small contribution of a hard-sphere structure factor $S(Q)$ for the systems in methylcyclohexane and TES (consistent with the plateaus in the profiles in the low Q region 0.08 $Å^{-1}$), indicative of weakly or non-interacting spherical droplets.[48] It is to note that these profiles could also be adequately fitted to the polydisperse sphere form factor $P(Q)$ only (excluding hard-sphere $S(Q)$) – consistent with the droplets being only very weakly/non-interacting (Table S4 in the SI lists the fit parameters, either with or without including hard-spheres $S(Q)$ in the model).

Table 1 lists the fitted parameters from these SANS data analyses. In the case of core-contrast samples, the fitted parameters were D_2O volume fraction ϕ_{D_2O}, droplet-core radius R_c^{av} and droplet polydispersity (PD) σ/R_c^{av} – where σ is a width factor accounting for the distribution of droplet radius (the fitted ϕ_{D_2O} values were within ±5% uncertainty with reference to values calculated based on known sample compositions). The AOT–SiC μE SANS profiles in methylcyclohexane and TES are broadly reminiscent of those obtained previously with standard AOT1-based W/O-μEs in *n*-heptane or cyclohexane,[4,43,49] which too can be modeled as non-interacting/weakly-interacting polydisperse spherical droplets.

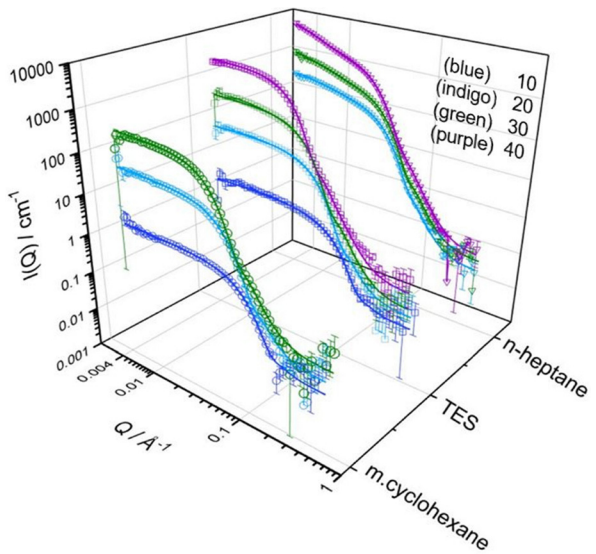

Fig. 5 Core-contrast (D_2O/h-surf/h-oil: D/H/H) SANS profiles for AOT–SiC W/O-μEs at [AOT–SiC] = 0.050 M and various W values in methylcyclohexane, triethylsilane (TES) and *n*-heptane. The solid lines represent fits to models described in the text and SI S.3. For better visualization the data and fits were multiplied by – (purple) × 11.7, (green) × 6, and (indigo) × 3 (the indigo data and solid lines (fits) in *n*-heptane are for W = 25).

For AOT–SiC μEs in *n*-heptane, however, there is a noteworthy increase of $I(Q)$ over the low Q region, consistent with interactions. Trial fits employing various models were performed on these profiles obtained in *n*-heptane to establish the most self-consistent account for $I(Q)$. These models accounted for scattering from cylindrical or ellipsoidal droplets, and spherical droplets with either a square-well $S(Q)$[50] or an Ornstein–Zernicke (OZ)[51] type $S(Q)$. The most physically reasonable and representative model was found to be for polydisperse spherical droplets with OZ-type $S(Q)$, which

Table 1 Fitting parameters for the SANS profiles in Fig. 5[a]

W ([water]/[surf])		5	10	20	25	30	40
R_c^{av}/Å	M. cyclohexane	18	23	36	—	48	—
	TES	—	20	36	—	47	68
	n-Heptane	17	—	—	42	46	55
PD, σ/R_c^{av}	M. cyclohexane	0.15	0.19	0.20	—	0.22	—
	TES	—	0.29	0.24	—	0.26	0.26
	n-Heptane	0.15	—	—	0.27	0.27	0.26
Correlation length, ξ/Å	M. cyclohexane	—	—	—	—	—	—
	TES	—	—	—	—	—	—
	n-Heptane	90 ± 10	—	—	129 ± 9	157 ± 14	222 ± 26

[a] SANS profiles corresponding to W = 5 systems are shown in Fig. S5, SI; uncertainty related to R_c^{av}: ± (1–2) Å; uncertainty related to PD: ± (0.01–0.03).

accounts for mild attractive interdroplet interactions (eqn (1))

$$S(Q) = 1 + \left[\frac{S(0)}{1 + (\xi Q)^d}\right] \quad (1)$$

where d = 2, $S(0)$ is the so-called compressibility factor linked to the droplet number-density over the correlation length ξ – and is a measure of interdroplet attraction strength. Previous work[43] suggested that cylindrical droplets are associated with viscous W/O-μEs: visual observations and mechanical stirring indicated only low viscosities for these AOT–SiC W/O-μEs, tending to rule out formation of extended cylindrical reversed micelles. The square well $S(Q)$ model (described in the SI) did not converge with the measured low-Q data. Hence, taking into account that previous analyses of W/O-μEs containing AOT1-analogues settled on the OZ- model,[43,52] it is reasonable to apply it here also.

Table 1 suggests that upon swelling the droplets by increasing W, the correlation length ξ values increase. Interestingly, these increases resemble AOT1-based W/O-μEs in *n*-decane (SI, Fig. S3)[53,54] having similar (or close) W compositions. An example comparison between the fitted functions for $S(Q)$ from these two different μEs at W = 30 is shown in Fig. S4 (SI). Of further note is how the two different systems are located close to their respective L_2-to-cloudy phase boundaries (T_U) (Fig. S2, SI): the phase behavior and the SANS profiles of these two chemically different systems are rather similar.

The SANS profiles of AOT–SiB W/O-μEs in toluene are shown in Fig. 6. These profiles share similar characteristics to that of AOT–SiC W/O-μEs in methylcyclohexane and TES (Fig. 5), which fit well to the polydisperse sphere $P(Q)$ (no structure factor), hence pointing to surfactant–solvent tunability, *i.e.*, similar droplets (oil–water interfaces with similar morphology) with variable surfactant–solvent combinations.

b. Headgroup (interfacial) area. To quantify adsorption at the W/O-μE interface, the molecular area per surfactant hydrophilic headgroup (a_h) was estimated by the swelling law[48] –

$$\alpha\left(\frac{\sigma}{R_c^{av}}\right) R_c^{av} = \frac{3v_w}{a_h} W + \frac{v_h}{a_h} \quad (3)$$

where v_w and v_h are the volumes of a water molecule (~30 Å^3) and surfactant headgroup respectively, and for Schulz

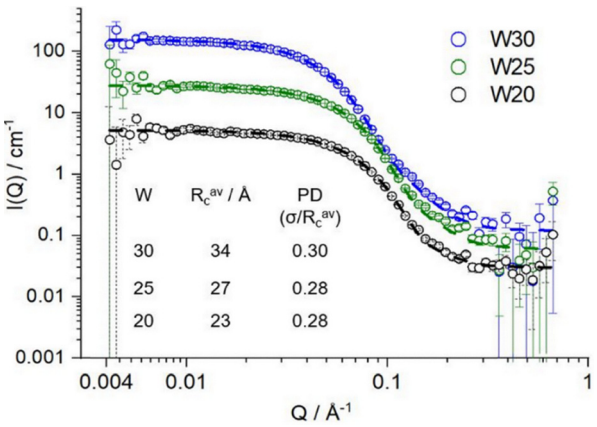

Fig. 6 Core-contrast SANS profiles (D_2O/H-surf//H-oil: D/H/H) for AOT–SiB W/O-μEs in toluene, [surf] = 0.050 M, temperature: 298 K; data and fits to the polydisperse $P(Q)$ model (dashed lines) were multiplied by (blue) × 6 and (green) × 3 for better visualization.

polydispersity, $\alpha\left(\frac{\sigma}{R_c^{av}}\right) = 1 + 2\left(\frac{\sigma}{R_c^{av}}\right)^2$. Assuming that the polydispersity is independent of W,[4] the slope of the swelling plot gives a_h and v_h values. The droplets swell in direct proportion to the composition W: R_c^{av} increases with W.[4]

Fig. 7 shows the droplet swelling plot corresponding to the AOT–SiC W/O-μEs discussed in the previous section; the inset lists a_h values. For reference, with AOT1-based systems in *n*-heptane[4,33] and methylcyclohexane (Fig. S6 in SI) the swelling-law derived values for a_h were 73–74 (± 2) Å^2. Therefore, the AOT1 and AOT–SiC interfacial areas per molecule are quite comparable.

c. Shell thicknesses. Simultaneous core–shell contrast[5,48] SANS measurements were carried out (shell contrast: D_2O/H-surf/D-oil: D/H/D) to obtain structural details about both the internal water droplet cores and the surfactant shell-thickness, t_s. Section S.3b(i) in the SI details the fitting models, and Fig. S7 show the simultaneously fitted core–shell profiles for AOT–SiC W/O-μEs in *n*-heptane and methylcyclohexane (W = 30). The core–shell fitted R_c^{av} values (44–46 Å) are quite comparable to those obtained with the complementary core-contrast R_c^{av} listed in Table 1. The fitted t_s values for each of the AOT–SiC hydrophobic tails were 9.4–9.5 (± ~0.5) Å, which is close to

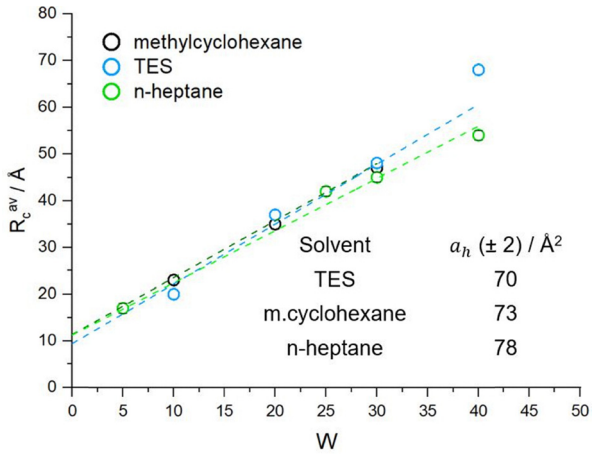

Fig. 7 Swelling-law plot for AOT–SiC W/O-μEs in methylcyclohexane, TES and *n*-heptane; uncertainties in R_c^{av}: ± 1 Å; solid lines are fits to eqn (3).

the calculated AOT–SiC chain length (the C–Si–C–C–C– backbone is ∼8.7 Å based on the sum of C and Si covalent radii[55]). These fitted t_s values are comparable to the previously resolved shell thickness of AOT1[4] (9.2 Å, theoretical chain backbone ∼9.2 Å), for instance, which suggests that the interfacial films constituted by the AOT–SiC and the benchmark AOT1 backbones are similar.

4. Discussion

4.1. General characteristics

The phase behavior (Fig. 3) is consistent with hydrophobic tail length being the dominant factor for microemulsifying capacity. Of the TMS surfactants introduced here, AOT–SiA is the least efficient for μE stabilization likely due to its very short chain backbone. Furthermore, AOT–SiB shows limited microemulsifying efficiency. As the phase diagrams indicate, AOT–SiB may be analogous to AOT–Phe[33] with a slight advantage in that the former is somewhat more μE-compatible with solvent blends containing linear *n*-alkanes. The AOT–SiB seems to be less solvent specific than AOT–Phe – which may be associated with the chain-tip nature (phenyl rings *vs.* branched trimethylsilyl moieties).[33]

As suggested by the core-contrast SANS results (Fig. 5), structurally, TMS surfactant-based W/O-μEs are like the AOT1 systems in solvents such as cyclohexane[49] (Fig. S6), *n*-heptane[4] or *n*-decane.[53,56] The droplets are polydisperse spherical, with or without weak interdroplet attractions, depending on the solvent. The swelling law derived a_h values suggest that the solvent (and the surfactant tail-backbone) chemical identities have only limited effects on interfacial packing (a_h values span 70–78 ± 2 Å²). In other words, AOT–SiC or AOT–SiB does not seem to exhibit any strikingly unique interfacial characteristics.

4.2. Interfacial efficiency: comparing silicone and fluorocarbon surfactants

The high salt branch of the electrolyte-scan IFT profiles (Fig. 4) suggests that the interfacial activity of AOT–SiC is similar to the previously reported AOT1-analogues with branched chain architectures.[26] The lowest $\gamma_{o/w}$ (*n*-heptane as the oil solvent) by AOT–SiC could be achieved as $\sim 8 \times 10^{-4}$ mN m^{-1}–which is comparable to the branched AOT1-analogues.[26,47] In particular, the IFT profile of AOT–SiC can be compared to the trimethyl chain-tip containing AOT3[26] – notably, both surfactants are structurally similar (Fig. S8, SI)–the water–*n*-heptane IFT profiles for these two surfactants almost overlap. Despite being super-efficient surfactants at the air–water surface, when it comes to O–W interfaces – the TMS surfactants seem to be more comparable to their hydrocarbon counterparts.[26,47]

To understand whether the TMS-surfactants are indeed viable alternatives for practical applications to fluorocarbon FSURFs and siloxane surfactants, the interfacial activities of TMS-surfactants have been compared in Table 2. This Table 2 lists *n*-heptane–water (model O–W interface) interface properties of AOT–SiC as well as for a collection of previously reported FSURFs[57–61] and silicone surfactants[62–64] (*n*-heptane is considered as a model oil). Some of these surfactants are commercially relevant: Capstone, for example, is used for generating fire-fighting foams.[8,57] Based on these values, it appears that AOT–SiC can be as efficient, if not more, as those other classes in lowering $\gamma_{o/w}$ and hence stabilizing O–W interfaces. The stabilization is comparable to the fluoroalkane – water $\gamma_{o/w}$, lowering of FSURFs to ∽1.0–5.0 mN m^{-1} (ref. 57 and 58) (for context, fluoroalkanes and FSURFs are chemically analogous; as a result, FSURFs stabilize fluoroalkane–water interfaces more effectively than hydrocarbon–water interfaces[57]). On the other hand, literature interfacial tensiometry data on siloxane surfactants at silicone oil–water interfaces is only limited; however, the microemulsification of silicone oil by these surfactants is well-known.[21,27,44,45,65,66] Therefore, it is safe to assume that siloxane surfactants would lower the $\gamma_{o/w}$ to the same extent as AOT–SiC. As Table 3 suggests, AOT–SiC is super-efficient along a wide-range of O–W interfaces (silanes and hydrocarbon solvents). Recently, Hinnant *et al.*[67] utilized machine learning to compile the surface and interface efficiency of tens of low energy FSURFs and siloxane surfactants. The majority of these surfactants lowered the $\gamma_{o/w}$ value (the oils varying from linear *n*-heptane to jet fuel mixes) up to 1–10 mN m^{-1}, which suggests that AOT–SiC is comparable with some of these commercially available FSURFs and siloxane surfactants. Importantly, the synthetic simplicity of AOT–SiC, chemical stability (*e.g.*, the absence of –OH groups), and its ability to form W/O-μEs (*i.e.*, achieving ultra-low $\gamma_{o/w}$, Fig. 4) distinguish this TMS surfactant as a potential next generation stabilizer over chemically unstable[21] and synthetically more involved[21,62,63] siloxanes and toxic[10,13–16] FSURFs.

5. Conclusion

This work demonstrates that the Si-containing TMS-hedgehog surfactants can stabilize oil–water (O–W) interfaces for efficient W/O-microemulsification, similarly to the benchmark dichain AOT1 and its branched hydrocarbon analogues.[4,26,31–33,69]

Table 2 Comparison of the performance of AOT–SiC to siloxane surfactants (or mixtures) and FSURFs at the *n*-heptane–water interface (without electrolyte); *n*-heptane is chosen as model oil; temperature = 298 K. The concentrations of surfactants (or mixes) are shown in parentheses

Surfactant	$\gamma_{o/w}$/mN m^{-1}	Ref.
AOT–SiC	1.25 ($>2\times$ cmc)	This work
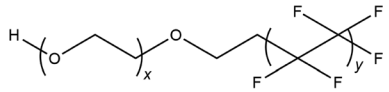 Capstone FS-30	5.2 (—)	57
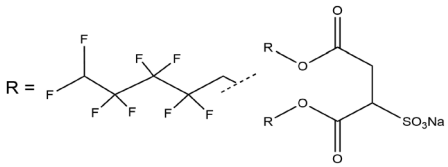 DiHCF4	6.2[a] (—)	58
equimolar mixture of C_4FI and C_3F_7COONa 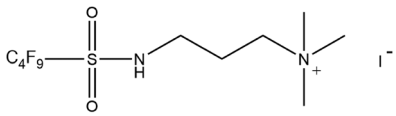 C_4FI	1.8 (30 mM)	59
mixture of Capstone® and Triton X-100 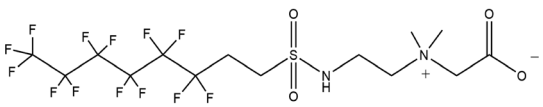 Capstone® 1157	2.9–3.8[b] (—)	60
surfactant mix containing fluorocarbon betaines or sulfobetaines 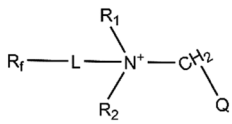 R_f = $(CF_2)_n$, n = 5-13; L = (-CHF), $(-CH_2)_2$ or $(-CH_2)_3$; R_1 or R_2 = $(-CH_2)_n$, n = 1-4, Q = COO^- or SO_3^-	1.0–2.4[c] (3 wt%)	61
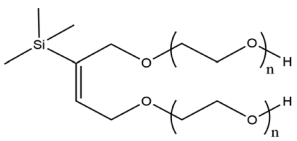 α,α'[2-(1,1,1,3,5,5,5-heptamethyltrisiloxan-3-yl)but-2-ene-1,4-diyl]-bis[ω-hydroxy-oligo(oxyethylene)]	1.0–6.0[d] (—)	62
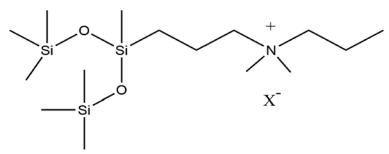 Branched trisiloxane	1.0 (>0.02 mM)	63

Table 2 (*continued*)

Surfactant	$\gamma_{o/w}$/mN m^{-1}	Ref.
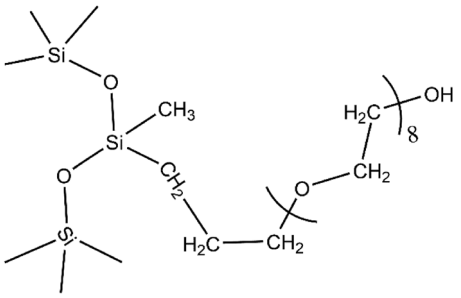 Linear Trisiloxane with branched chain-tip (D-8)	0.03[e] (∼ 8 mM)	64

[a] cmc of AOT–SiC = 2.52 mM (SI); $\gamma_{o/w}$ was calculated using the following equation $R_{IFT} = 1 - (\gamma_{o/w\,no\,surf.} - \gamma_{o/w}/\gamma_{o/w\,no\,surf.})$, where R_{IFT} is taken from ref. 58, $\gamma_{o/w\,no\,surf.}$ is the interfacial tension of a pure *n*-heptane–water interface (no surfactant). The $\gamma_{o/w\,no\,surf.}$ value was taken from ref. 68. [b] Range of values depending on variable molar ratios. [c] Tap or sea water. [d] Range of values depending on the degree of ethoxylation. [e] *n*-Hexane.

Table 3 Oil–water interfacial tension values of AOT–SiC under salt-free conditions

Solvent	$\gamma_{o/w}$ (± 0.01)/mN m^{-1}
n-Heptane	1.25
Toluene	0.45
Methylcyclohexane	0.74
Triethylsilane	0.87

Moreover, as suggested previously,[4,32,69] "brushlike" trimethyl branched chain-tips may indeed facilitate microemulsification for the TMS surfactants like the branched hydrocarbon analogues. The phase diagrams indicate that AOT–SiC surfactants, like AOT1, can stabilize microemulsions (μEs) in saturated hydrocarbon solvents that may or may not contain Si-atoms, and that AOT–SiB exhibits solvent-specific microemulsification, just like the phenyl-tipped AOT–Phe.[33] The high-salt branch IFT profiles show that these TMS-hedgehog surfactants exhibit ultralow $\gamma_{o/w}$s, and that these IFT profiles are comparable to those[26] shown by AOT1 and its branched hydrocarbon analogues. For AOT–SiC, the minimum $\gamma_{o/w}$ of $\sim 8 \times 10^{-4}$ mN m^{-1} was achieved. Model fitting analysis of contrast-variation SANS experiments indicated spherical polydisperse surfactant-coated nanodroplets in these systems. In this regard, the TMS surfactants are quite similar to the standard hydrocarbon AOT1 analogues.[4,26,33] In terms of lowering $\gamma_{o/w}$, AOT–SiC appears to be at least as efficient as certain fluorinated FSURFs[57–61] and siloxanes.[62–64] Additionally, the high microemulsification capacity (especially for AOT–SiC) and the less complicated synthesis suggest that this TMS class is a viable alternative to siloxane and FSURFs for industrial applications.[70] Further work may involve counterion variation with AOT–SiC to achieve even higher surface activity[71] and studies of the μEs. It is known that counterions such as Ni^{2+} and Co^{2+} for AOT1 result in cylindrical reverse micelles in oil-solvents;[48] and so, it will be interesting to explore this possibility with TMS surfactants, offering possible new applications in high performance engine additives.[72] The hydrophobic chains can be further modified too. The simplest way to do so and achieve higher efficiency is by increasing the hydrophobic chain alkyl carbon number. The effect of C atom inclusion on the interfacial performance of TMS derivatives was already noted in this work. Another strategy may involve extending the di-chain architecture to tri-chains. Such tri-chain TMS surfactants showed enhanced CO_2 thickening properties;[24] they can be explored for O–W interface stabilization too. The chain-tips in dichain derivatives can be "elongated" by incorporating longer alkyl groups covalently bonded to the Si chain-tip atoms. Another way to achieve more enhanced interfacial activity may be incorporating multiple Si atoms on each of the hydrophobic chains (*e.g.*, tris(trimethylsilyl) groups). These new, exotic silyl surfactants could be readily synthesized by using the corresponding precursor alcohols and following the synthetic protocol of AOT–SiC, for example. In short, pushing the boundary for versatile design and synthesis of chemically stable, super-efficient alkylsilyl surfactants is feasible.

Author contributions

A. R.: experiments (synthesis, phase behavior, tensiometry, SANS), data acquisition, analysis and fitting, writing and reviewing the original draft, editing, responding to the reviewers' comments; J. E.: supervision, SANS beamtime acquisition, writing and reviewing the original draft, editing, responding to the reviewers' comments; G. L. M., I. E. S., D. M. K., and S. S.: experiment (SANS), discussion on data; S. E. R. and R. M. D.: SANS instrument responsibles (SANS2D and Larmor respectively); S. P.: SANS instrument (D11, ILL) responsible, editing.

Conflicts of interest

There are no conflicts to declare.

Data availability

The data supporting this article have been included as part of the supporting information (SI). Supplementary information is available. See DOI: https://doi.org/10.1039/d5sm00817d.

Acknowledgements

A. R. thanks the Commonwealth Scholarship Commission in the UK for a PhD scholarship. ISIS Neutron and Muon Sources of STFC and Institut Laue-Langevin (ILL, France) are thanked for beamtime, travel, grants, and consumables. Part of this work was based on results presented in the PhD thesis of A. R.[73]

References

1 A. Czajka, G. Hazell and J. Eastoe, *Langmuir*, 2015, **31**, 8205.
2 J. Eastoe, A. Downer, A. Paul, D. C. Steytler, E. Rumsey, J. Penfold and R. Heenan, *Phys. Chem. Chem. Phys.*, 2000, **2**, 5235.
3 G. N. Smith, P. Brown, C. James, S. E. Rogers and J. Eastoe, *Colloids Surf., A*, 2016, **494**, 194.
4 S. Nave, J. Eastoe, R. K. Heenan, D. C. Steytler and I. Grillo, *Langmuir*, 2000, **16**, 8741.
5 S. Nave, J. Eastoe and J. Penfold, *Langmuir*, 2000, **16**, 8733.
6 Fluorinated surfactant market insight, https://www.fortunebusinessinsights.com/fluorosurfactant-market-102344, (accessed December 2024).
7 https://www.ictchemicals.com/products/technical-platforms/fluorinated-surfactants/ (accessed on August 2024).
8 C. Hill, A. Czajka, G. Hazell, I. Grillo, S. E. Rogers, M. W. Skoda, N. Joslin, J. Payne and J. Eastoe, *J. Colloid Interface Sci.*, 2018, **530**, 686.
9 M. P. Krafft, *Adv. Drug Delivery Rev.*, 2001, **47**, 209.
10 K. J. Harris, G. Munoz, V. Woo, S. Sauve and A. A. Rand, *Environ. Sci. Technol.*, 2022, **56**, 14594.
11 J. Giesy and K. Kannan, *Environ. Sci. Technol.*, 2002, **36**, 146A.
12 Toxicity of perfluoroalkyl substances, https://www.atsdr.cdc.gov/toxprofiles/tp200.pdf, (accessed October 2024).
13 *Toxicological Effects of Perfluoroalkyl and Polyfluoroalkyl Substances*, ed. J. C. DeWitt, Springer International Publishing, Switzerland, 2015.
14 Z. Wang, J. C. DeWitt, C. P. Higgins and I. T. Cousins, *Environ. Sci. Technol.*, 2017, **51**, 2508.
15 PFAS forever chemicals, https://www.theguardian.com/fashion/2021/jun/15/pfas-makeup-forever-chemicals, (accessed August 2024).
16 K. F. Kwiatkowski, D. Q. Andrews, L. S. Birnbaum, T. A. Bruton and J. C. DeWitt, *et al.*, *Environ. Sci. Technol. Lett.*, 2020, **7**, 532.
17 https://news.bloomberglaw.com/environment-and-energy/pfas-bans-restrictions-go-into-effect-in-states-as-year-begins, (accessed August 2024).
18 United Nations Environment Programme, Stockholm Convention, https://www.pops.int/TheConvention/ThePOPs/AllPOPs/tabid/2509/Default.aspx, (accessed November 2024).
19 Registry of restriction intensions until outcome, https://echa.europa.eu/registry-of-restriction-intentions/-/dislist/details/0b0236e18663449b, (accessed December 2024).
20 R. Ananth, A. Snow and K. Hinnant, *et al.*, *Colloids Surf., A*, 2019, **589**, 123686.
21 R. Hill, in *Specialist Surfactants*, ed. I. D. Robb, Springer, Dordrecht, 1st edn, 1997, ch. 6, p. 143.
22 G. Ramis-Ramos, E. F. Simo-Alfonso, A. Escrig-Domenech and M. Beneito-Cambra, Liquid chromatography of surfactants, *Reference module in chemistry, molecular sciences and chemical engineering*, Elsevier, Amsterdam, 2016.
23 A. Czajka, C. Hill, J. Peach, J. C. Pegg, I. Grillo, F. Guittard, S. E. Rogers, M. Sagisaka and J. Eastoe, *Phys. Chem. Chem. Phys.*, 2017, **19**, 23869.
24 C. Hill, Y. Umetsu, K. Fujita, T. Endo, K. Sato, A. Yoshizawa, S. E. Rogers, J. Eastoe and M. Sagisaka, *Langmuir*, 2020, **36**, 14829.
25 J. Eastoe, in *Colloid science principles, methods and applications*, ed. T. Cosgrove, Wiley, New York, 2nd edn, 2010, ch. 4, p. 61.
26 S. Nave, J. Eastoe, R. K. Heenan, D. C. Steytler and I. Grillo, *Langmuir*, 2002, **18**, 1505.
27 R. M. Hill, *Silicone surfactants*, Routledge, New York, 1999.
28 H. Kunieda, H. Taoka, T. Iwanaga and A. Harashima, *Langmuir*, 1998, **14**, 5113.
29 M. S. Ferreira, H. Westfahl Jr and W. Loh, *Langmuir*, 2019, **123**, 10522.
30 S. C. Sharma, K. Tsuchiya, K. Sakai, H. Sakai, M. Abe, S. Komura, K. Sakamoto and R. Miyahara, *Langmuir*, 2008, **24**, 7658.
31 J. Eastoe, B. H. Robinson, D. C. Steytler and D. Thorn-Leeson, *Adv. Colloid Interface Sci.*, 1991, **36**, 1.
32 L. Hudson, PhD thesis, University of Bristol, 2008.
33 S. Nave, A. Paul, J. Eastoe, A. R. Pitt and R. K. Heenan, *Langmuir*, 2005, **21**, 10021.
34 P. D. Fletcher, A. M. Howe and B. H. Robinson, *J. Chem. Soc., Faraday Trans.*, 1987, **83**, 985.
35 C. D. Dewhurst, I. Grillo, D. Honecker, M. Bonnaud, M. Jacques, C. Amrouni, A. Perillo-Marcone, G. Manzin and R. Cubitt, *J. Appl. Crystallogr.*, 2016, **49**, 1–14.
36 R. K. Heenan, S. E. Rogers, D. Turner, A. E. Terry, J. Treadgold and S. M. King, *Neutron News*, 2011, **22**, 19–21.
37 C. D. Dewhurst, *J. Appl. Crystallogr.*, 2023, **56**, 1595–1609.
38 O. Arnold, J. C. Bilheux, J. M. Borreguero, A. Buts and S. I. Campbell, *et al.*, *Nucl. Instrum. Methods Phys. Res., Sect. A*, 2014, **764**, 156–166.
39 https://www.sasview.org/.
40 F. D. Blum, S. Pickup, B. W. Ninham, S. J. Chen and D. F. Evans, *J. Phys. Chem.*, 1985, **89**, 711.
41 M. Olla and M. Monduzzi, *Langmuir*, 2000, **16**, 6141.
42 M. P. Pileni, *J. Phys. Chem.*, 1993, **97**, 6961–6973.
43 O. Myakonkaya, J. Eastoe, K. J. Mutch, S. Rogers, R. Heenan and I. Grillo, *Langmuir*, 2009, **25**, 2743.

44 X. Li, R. Washenberger, L. E. Scriven, H. T. Davis and R. M. Hill, *Langmuir*, 1999, **15**, 2267.
45 X. Li, R. Washenberger, L. E. Scriven, H. T. Davis and R. M. Hill, *Langmuir*, 1999, **15**, 2278.
46 D. C. Steytler, D. L. Sargeant, B. H. Robinson, J. Eastoe and R. K. Heenan, *Langmuir*, 1994, **10**, 2213.
47 B. P. Binks, H. Kellay and J. Meunier, *Europhys. Lett.*, 1991, **16**, 53.
48 J. Eastoe, *Surfactant chemistry*, Wuhan University Press, China, 2005.
49 J. Eastoe, G. Fragneto, B. H. Robinson, T. F. Towey, R. K. Heenan and F. Leng, *J. Chem. Soc., Faraday Trans.*, 1992, **88**, 461.
50 R. V. Sharma and K. C. Sharma, *Physica*, 1977, **89A**, 213.
51 L. S. Ornstein and F. Zernike, *Proct. Sect. Sci. K. Med. Akad. Wet.*, 1914, **17**, 793.
52 S. Nave, PhD Doctoral thesis, University of Bristol, 2001.
53 J. S. Huang, *J. Chem. Phys.*, 1985, **82**, 480.
54 S. H. Chen, *Phys. B*, 1986, **137**, 183.
55 S. S. Zumdahl and S. A. Zumdahl, *Chemistry*, Brooks/Cole, California, 8th edn, 2010.
56 M. Kotlarchyk, J. S. Huang and S. H. Chen, *J. Phys. Chem.*, 1985, **89**, 4382.
57 V. Trinh, C. S. Malloy, T. J. Durkin, A. Gadh and S. Savagatrup, *ACS Sens.*, 2022, **7**, 1514.
58 R. F. Tabor, S. Gold and J. Eastoe, *Langmuir*, 2006, **22**, 963.
59 Y. He, Q. Sun, H. Xing, Y. Wu and J. Xiao, *J. Dispersion Sci. Technol.*, 2019, **40**, 319.
60 K. M. Hinnant, S. L. Giles, A. W. Snow, J. P. Farley, J. W. Fleming and R. Ananth, *J. Surfactants Deterg.*, 2018, **21**, 711.
61 K. P. Clark and E. K. Kleiner, *European Pat.*, EP0774998B1, 2000.
62 R. Wersig, G. Sonnek and C. Niemann, *Appl. Organomet. Chem.*, 1992, **6**, 701.
63 G. Schmaucks, G. Sonnek, R. Wustneck, M. Herbst and M. Ramm, *Langmuir*, 1992, **8**, 1724.
64 T. Svitova, H. Hoffmann and R. M. Hill, *Langmuir*, 1996, **12**, 1712.
65 R. M. Hill, *Curr. Opin. Colloid Interface Sci.*, 2002, **7**, 255.
66 R. M. Hill, *US Pat.*, 5705562, 1998.
67 K. M. Hinnant, P. E. Sudol, J. A. Kramer, D. W. Moore, L. C. Brown, C. M. Bunton, M. C. Davis, A. W. Snow and R. Ananth, *ACS Omega*, 2025, **10**, 42270.
68 A. Goebel and K. Lunkenheimer, *Langmuir*, 1997, **13**, 369.
69 J. Eastoe, A. Paul, S. Nave, D. C. Styetler, B. H. Robinson, E. Rumsey, M. Thorpe and R. K. Heenan, *J. Am. Chem. Soc.*, 2001, **123**, 988.
70 M. Sagisaka, T. Darmanin, F. Guittard and J. Eastoe, *J. Colloid Interface Sci.*, 2025, **690**, 137229.
71 M. Sagisaka, T. Endo, K. Fujita, Y. Umetsu, S. Osaki, T. Narumi, A. Yoshizawa, A. Mohamed, F. Guittard, C. Hill and J. Eastoe, *Colloids Surf., A*, 2021, **631**, 127690.
72 G. Moody, PhD Doctoral thesis, University of Bristol, 2023.
73 A. Rahman, PhD Doctoral thesis, University of Bristol, 2023.

